Shimabukuro, K., et al. Reconstitution of amoeboid motility in vitro identifies a motor-independent mechanism for cell body retraction

Supplemental information

Supplemental Data:

1. Movie S1, related to Figure 1. Growth of a conventional MSP fiber in 20% S100 plus 1 mM ATP. The fiber elongates by assembling filaments at the vesicle but does not exhibit disassembly or retraction.

2. Movie S2, related to Figure 1. An MSP comet tail fiber that grows at its vesicle-bearing end and disassembles rearward like the actin comet tails that form behind some intacellular pathogens or beads coated with activators of actin nucleators.

3. Movie S3, related to Figure 1. A comet tail fiber pulling a load. This time lapse sequence of the fiber shown in Figure 1B shows the rear of the fiber picking up a clump of debris at the start of the sequence and pulling it forward for about 8 min indicating that retraction generates sufficient force to perform work.

4. Movie S4, related to Figure 1. The full time lapse sequence, shown in part in Figure 1C, of a comet tail fiber labeled with Cy3-MSP fluorescent speckles.

5. Figure S1, related to Figure 1.

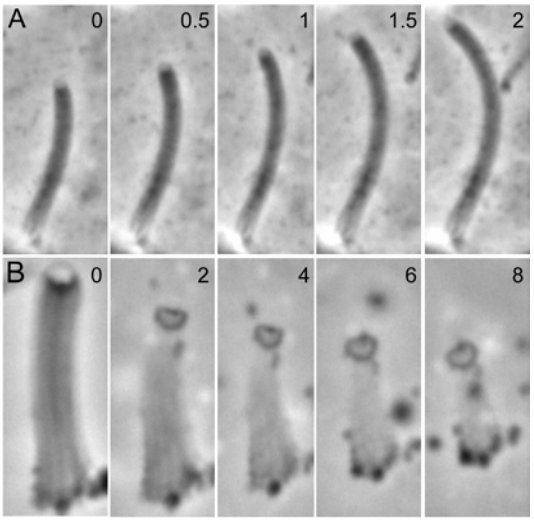

Figure S1. Reconstitution of protrusion and retraction independently in conventional MSP fibers. (A) Time lapse sequence of a conventional fiber grown in five-fold diluted S100 with 1 mM ATP. Elongation of the fiber pushes the plasma membrane-derived vesicle forward recapitulating the events associated with

leading edge protrusion in crawling sperm. (B) A conventional fiber retracting following treatment with S100 supplemented with tyrosine phosphatase, YOP. These conditions trigger retraction but stop fiber growth so that protrusion no longer occurs.

6. Figure S2, related to Figure 4.

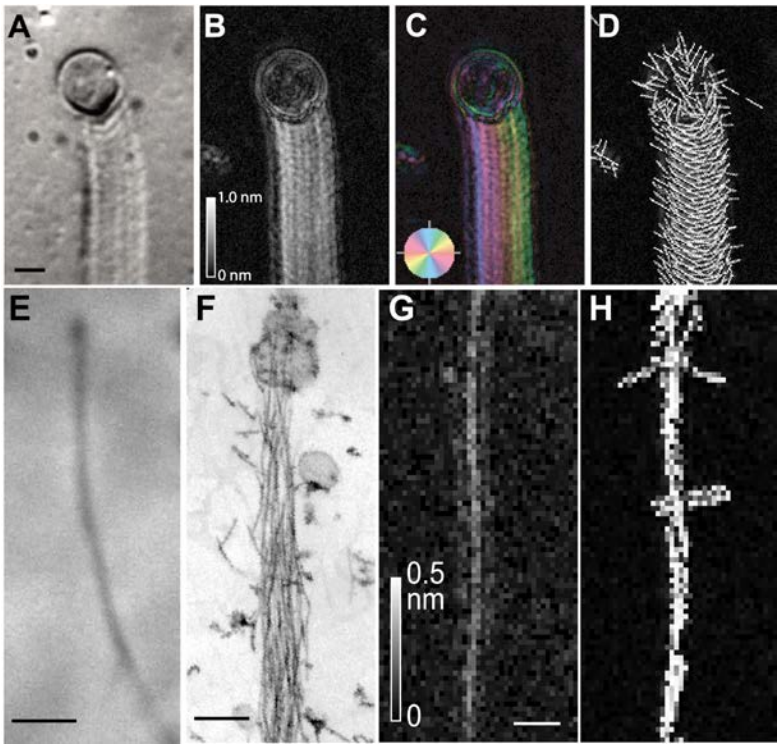

Figure S2. Panels A-D: Explanation of the computed images obtained by LC Polscope microscopy using a MSP fiber as an example. Fiber viewed in (A) DIC optics, (B) the corresponding computed retardance image, (C) a computed image showing the slow axis by color coding of the orientation (D) diagram showing the orientation of the slow axis as lines. The appearance of different fibers under DIC optics varied considerably but most commonly included longitudinal stripes along the fiber axis as shown in A. The LC-Polscope uses a combination of liquid crystal electro-optical modulators and image processing software to measure the magnitude of the retardance and the orientation of the slow axis of birefringence at every pixel in an image. Thus, the LC-Polscope produces computed images that show the magnitude of retardance at each pixel as shades of gray (see Figure 5b) and the orientation of birefringence displayed as a series of lines (see Figure 5c). Bar = 2 **Panels E-H**: Calibration of the orientation of birefringence of MSP filaments against filament arrays of known orientation using images of MSP microfibers [S1]. (E) phase contrast image of a microfiber growing in S100. The growing end is marked by a membranous cap that appears as a small knob. (F) EM view of a thin section through the growing end of a microfiber showing that the shaft is comprised of a bundle of filaments most of which are aligned with the microfiber axis. Bar, 200 nm. (G) computed retardance image of a microfiber obtained by LC-Polscope microscopy. The microfiber is clearly visible in the retardance image, suggesting that microfiber is birefringent due to the highly aligned MSP filaments. Bar, 1 m. (H) line diagram of the birefringence orientation in a microfiber. Almost all lines are parallel to the long axis of the microfiber showing that the slow axis of birefringence is aligned with the axis of the filaments that comprise the microfiber. Thus, for MSP filaments, as for actin filaments and microtubules, the slow axis of the birefringence can be used to determine filament orientation.

Supplemental Experimental Procedures

Sperm collection and S100 preparation

Ascaris males were obtained from the intestines of infected hogs at Smithfield Packing Co., Inc (Smithfield, VA). Sperm were collected and activated as described [S2]. To prepare a cell-free extract, sperm were pelleted for 10 sec at 5000 g at room temperature. The supernatant was removed and the cell pellet was frozen at -70^{o}C, thawed on ice, centrifuged at 10,000 g for 10 min at 4ºC, and then spun at 100,000 g for 45 min at 4ºC in a TLA100.3 rotor in a tabletop ultracentrifuge (Beckman Instruments, Palo Alto, CA). The supernatant (S100) was used for motility assays.

Light microsocpy

To grow fibers, 2.5 μl of a solution containing 20 or 80 % S100 diluted in KPM buffer (0.5 mM $MgCl_2$, 10 mM potassium phosphate, pH 6.8), 1 mM sodium orthovanadate (OV), and the indicated concentration of ATP were pipetted onto a glass slide and covered with an 8 x 8 mm coverslip (VWR, West Chester, PA). These preparations were sealed with VALAP (a mixture of equal amounts of lanolin, Vaseline and paraffin) and examined on an Axioskop 2 plus microscope (Carl Zeiss, Inc., Thornwood, NY) equipped with a 40X phase contrast objective (N.A.=0.6). Time lapse images were acquired using a Hamamatsu ORCA-ER camera (Bridgewater, NJ) controlled by MetaMorph software (Molecular Devices, Sunnyvale, CA).

Fluorescence Speckle Microscopy

MSP was purified from *Ascaris* sperm as described [S3]. For labeling, purified MSP was mixed with Cy3-maleimide (GE Healthcare, Waukesha, WI) at 1:1.5 molar ratio in 16 mM HEPES-KOH (pH 7.5) and incubated for 1 hr at room temperature. After the removal of unreacted dye with a spin column (bio-rad, Hercules, CA), Cy3-labeled MSP was frozen with liquid nitrogen and stored at -70 C until use. The protein/dye ratio was 1:0.88. For fluorescence speckle labeling of fibers, we prepared 40 nM Cy3-MSP in 80 % S100 supplemented with 1 mM OV, 0.5 – 1 mM DTT, and the indicated concentration of ATP. Slides were prepared and examined as described above using a 60X objective (N.A.=1.4), an HQ TRITC filter set (Chroma Technology, Bellows Falls, VT), and an electric shutter system (UNIBLITZ VS35, Vincent Associates, Rochester, NY). Images were acquired at 5 sec intervals with an 800-ms exposure time. An unsharp mask was routinely applied to time lapse images to enhance the contrast of the fluorescent speckles.

Correlative confocal fluorescence and electron microscopy

Comet tail fibers were grown in 80% S100 containing 0.5 mM ATP, 1 mM OV, 0.5 mM DTT, and 57 μM Cy3-labeled MSP. To facilitate correlative microscopy, the fibers were grown in chambers formed by placing 2.5 μl of sample between two coverslips (8 x 8 mm and 18 x 18 mm) without spacers. After 14 min the chambers were transferred to a 10-ml beaker containing 6 ml of KPM, opened gently by allowing the smaller coverslip to fall off from the other coverslip, and fixed by adding 1.25 % glutaraldehyde to the beaker to a concentration of 1.25% for 20 minutes at room

temperature. DIC and fluorescence images of fixed fibers were taken with LSM 510 confocal laser scanning microscope (Carl Zeiss, Inc., Thornwood, NY) using a 60X objective and an appropriate filter set. To obtain the information about the filament distribution within the comet tail fiber, a series of fluorescent images along the z axis were taken at 0.41 μm intervals. Platinum replicas of these comet tail fibers were prepared as described previously [S4]. Replicas were examined with a Philips CM120 transmission electron microscope operated at 80 kV and images were acquired with Tem-Cam F244 slow scan CCD camera (TVIPS, Gauting, Germany). To investigate changes in the filament mass and the filament density along the length of the comet tail fiber, first a cross section of the comet tail fiber was generated from the fluorescence z-stack and the total fluorescence intensity was measured. The radius at the same position of the fiber was measured in the EM image. The fluorescence density, an estimate of the filament density, was determined at 1 μm interval along the length of the fiber by dividing the total fluorescence intensity in the cross section by the square of the fiber radius.

Electron Microscopic Tomography

For electron tomography, a grid containing a platinum replica of comet tail fibers was mounted on an ultrahigh tilt holder (Gatan Model 670, Pleasanton, CA). A tilt series of images were acquired over ±60° at 1 or 2° intervals using a Philips CM120 transmission electron microscope operated at 80 kV and equipped with a Tem-Cam F244 slow scan CCD camera. Image alignment and refinement and also the backprojection of the 3D map from the tilt series were performed by using Protomo, a tomography software package [S5]. The resulting 3D maps were imported into IMOD for further analysis. For the measurement of filament length, each filament in the 3D map was traced by hand using a modeling feature in IMOD [S6]. Only filaments in which both ends were clearly defined were used for length measurement. To measure filament packing density, a cuboid (0.5 μm in length, with its width and height set so that the cross-section of the fiber was included in the cuboid) containing a part of the comet tail fiber was cropped out from a 3D map and its position and orientation were adjusted so that the axis of the comet tail fiber was parallel to the length of the cuboid. After all filaments in the cuboid were traced and counted by hand, the filament density was determined by dividing number of filaments in the cuboid by the fiber volume, which was estimated by multiplying the length of the cuboid by the cross-sectional area of the comet tail fiber.

LC-PolScope Microscopy

Fibers prepared as described for other light microscopy techniques were examined using a Nikon microscope (microphot SA, Melville, NY) equipped with a 63x objective (NA=1.4), a CCD camera, a 2x intermediate lens, and the components used for LC-Polscope microscopy. The design and operation of the LC-PolScope are described in [23]. Briefly, the LC-PolScope is based on a traditional polarized microscope, but equipped with a universal compensator made from two liquid crystal devices instead of the crystal compensator (Cambridge Research and Instrumentation, Cambridge, MA). By controlling the electrical voltages applied to the liquid crystal devices, the LC-PolScope can create five different illumination conditions with different polarization states in quick succession during the image acquisition. PSj, a program bundled with LC-PolScope, was used to calculate the retardance and the orientation of the slow axis of the birefringence

from information in the five images. These parameters were displayed as independent computed images. The computed retardance image generated by the LC-PolScope is independent of the orientation of the sample and shows all anisotropic structures within the sample displayed in 8-bit grey scale. The orientation of the slow axis of the birefringence is shown as a line diagram in which lines showing the orientation of the slow axis of the birefringence were drawn for every fourth or fifth pixel in the image.

To analyze the filament orientation relative to the long axis of the fiber quantitatively, we prepared a pair of computer-generated images; one showed retardance and the other showed the orientation of the slow axis in grey scale instead of as a stick diagram. We defined corresponding regions of a comet tail fiber in both the retardance and orientation images, and extracted the grey scale values for retardance and orientation for all pixels in the region. We set the long axis of the comet tail fiber, determined by eye, as 0° and expressed the orientation angle of all slow axis data relative to this reference. We then sorted all pixels into groups based on their angle of orientation. To minimize the effect of background noise, we applied a retardance threshold (typically retrardance = 0.14 nm) to eliminate pixels with low retardance values from further analysis. The sum of the retardance of all remaining pixels in each orientation group was calculated and plotted as a function of angle relative to the long axis of the fiber.

Supplemental References:

S1. Miao, L., Yi, K., Mackey, J.M., and Roberts, T.M. (2007) Reconstitution in vitro of MSP-based filopodium extension in nematode sperm. Cell Motil Cytoskeleton *64*, 235-247.

S2. Sepsenwol, S., Ris, H., and Roberts, T.M. (1989) A unique cytoskeleton associated with crawling in the amoeboid sperm of the nematode, Ascaris suum. J Cell Biol *108*, 55-66.

S3. King, K.L., Stewart, M., Roberts, T.M., and Seavy, M. (1992) Structure and macromolecular assembly of two isoforms of the major sperm protein (MSP) from the amoeboid sperm of the nematode, Ascaris suum. J Cell Sci *101*, 847-857.

S4. Svitkina, T. (2007) Electron microscopic analysis of the leading edge in migrating cells. Methods Cell Biol *79*, 295-319.

S5. Winkler, H., and Taylor, K.A. (2006) Accurate marker-free alignment with simultaneous geometry determination and reconstruction of tilt series in electron tomography. Ultramicroscopy *106*, 240-254.

S6. Kremer, J.R., Mastronarde, D.N., and McIntosh, J.R. (1996) Computer visualization of three-dimensional image data using IMOD. J Struct Biol *116*, 71-76.